Supplementary information for

Urban greening effectively curbs warming in Chinese cities

Dong Xu (徐栋)[1,2,3] et al.

[1] State Key Laboratory of Remote Sensing Science, Faculty of Geographical Science, Beijing Normal University, Beijing 100875, China

[2] Institute of Remote Sensing Science and Engineering, Faculty of Geographical Science, Beijing Normal University, Beijing 100875, China

[3] Key Laboratory of Environmental Change and Natural Disasters of Ministry of Education, Beijing Normal University, Beijing 100875, China

This PDF file contains:

- Supplementary Text 1-5
- Supplementary Figures 1-9
- Supplementary Tables 1-4
- Graphic Abstract
- Abbreviations
- References

Supplementary Text 1-5

Supplementary Text 1 | Association of urban heatness, greenness and greyness at the cluster scale

Supplementary Text Fig. 1 shows the relationship between Sen_UST, Sen_NDVI and Sen_IBI at the cluster scale, aggregating the indicator interval information for 1804 urban clusters with an area greater than 10 km^2 (see Supplementary Table 2 for a breakdown by natural paragraph point method). Overall, there are 1041 urban clusters (57.71%) with Sen_NDVI > 0 (Supplementary Text Fig. 1a), and the national average greening trend was about $0.33 \pm 4.40\times10^{-3}$/yr (mean ± a STD). The clusters with the greatest greening were located in the Loess Plateau, Northwest China, the Southeast Coastal Region, and Northeast China. In contrast to the *UG*, the regions with pronounced *UI* growth were mainly located in the North China Plain, the Chengdu Plain, the Eastern Coastal Region, and South China (Fig. 2d). Similarly, the fastest-growing areas of UST were located in the Chengdu Plain, the North China Plain and Jiangsu Province (Fig. 2d).

The rapid decline of UG and the rise of UI will promote the continuous rise of the UST [1,2]. The mean Sen_NDVI of all urban clusters with U1 was $1.75 \pm 2.63\times10^{-3}$/yr, while the mean Sen_NDVI of all urban clusters with U5 was $-1.12 \pm 3.13\times10^{-3}$ /yr (Supplementary Text Fig. 1a). Second, the UG of 77.72% of urban clusters with U1 showed an upwards trend, while the UG of only 28.66% of urban clusters with U2 showed an upwards trend (Supplementary Text Fig. 1a). In the process of rapid urbanization, the UI of most urban clusters increased. There were the most urban clusters with Sen_IBI in the B3-B5 level, with a total of 1129 (62.58%). The mean Sen_IBI of all U1 urban agglomerations was $-2.66 \pm 2.44\times10^{-3}$ /yr, while the mean Sen_IBI of all U5 urban clusters was $2.66 \pm 1.56\times10^{-3}$/yr (Supplementary Text Fig. 1d). Moreover, the UI of 85.64% of urban clusters with U1 showed a downwards trend, while the UI of only 1.91% of urban clusters with U5 showed a downwards trend (Supplementary Text Fig. 1d). Different from previous studies [3], this shows that UST is significantly correlated with UG (negative correlation) and UI (positive correlation) in both spatial and temporal dimensions.

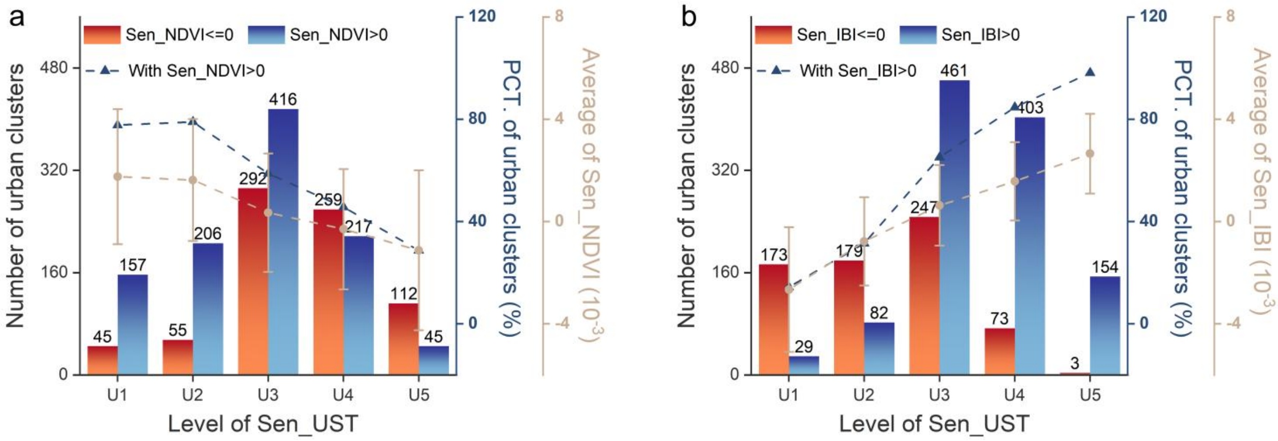

Supplementary Text Fig. 1 | Relationships between Sen_UST, Sen_NDVI and Sen_IBI at the cluster scale. a, Composite graph of the quantitative relationship between Sen_UST and Sen_NDVI at the cluster scale. b, Composite graph of the quantitative relationship between Sen_UST and Sen_IBI at the urban cluster scale.

Supplementary Text 2 | 'Greening' path towards the National Forest City of Karamay and Aksu

Since the completion of the water diversion project in 2000, Karamay has actively promoted UG construction. This initiative is evident through the annual April compulsory tree planting activities and key gardening projects (Supplementary Text Fig. 2). Karamay remains committed to constructing an attractive and habitable urban environment that meets its citizens' aspirations for a better quality of life. Presently, the city is experiencing a yearly 2% increase in its greening rate, and the vision of transforming Karamay into a "green city" is gradually becoming a reality. The green space in Karamay exceeded 31.62 km^2 in 2021, with a green coverage of 43.95% and 13.78 m^2 of parkland per capita. Supporting evidence from space imagery validates that Karamay's urban area has experienced continuous greening in the past two decades (Supplementary Text Fig. 3).

Notably, Aksu has the lowest urbanization level compared to the remaining 14 cities and sports a CPUG of 1.18 ± 2.99 K. Like Karamay, the driving force behind UG in Aksu is ecological restoration projects (ERPs) across China. It is an early example of a national forest city in Xinjiang [4], with the "Kökyar project" [5] being instrumental in urging locals to participate in tree planting over the last two decades. The project has resulted in the nurturing of a million acres of "green sea" in southern Xinjiang, earning it a position on the United Nations' "Global 500 Best Places" [6].

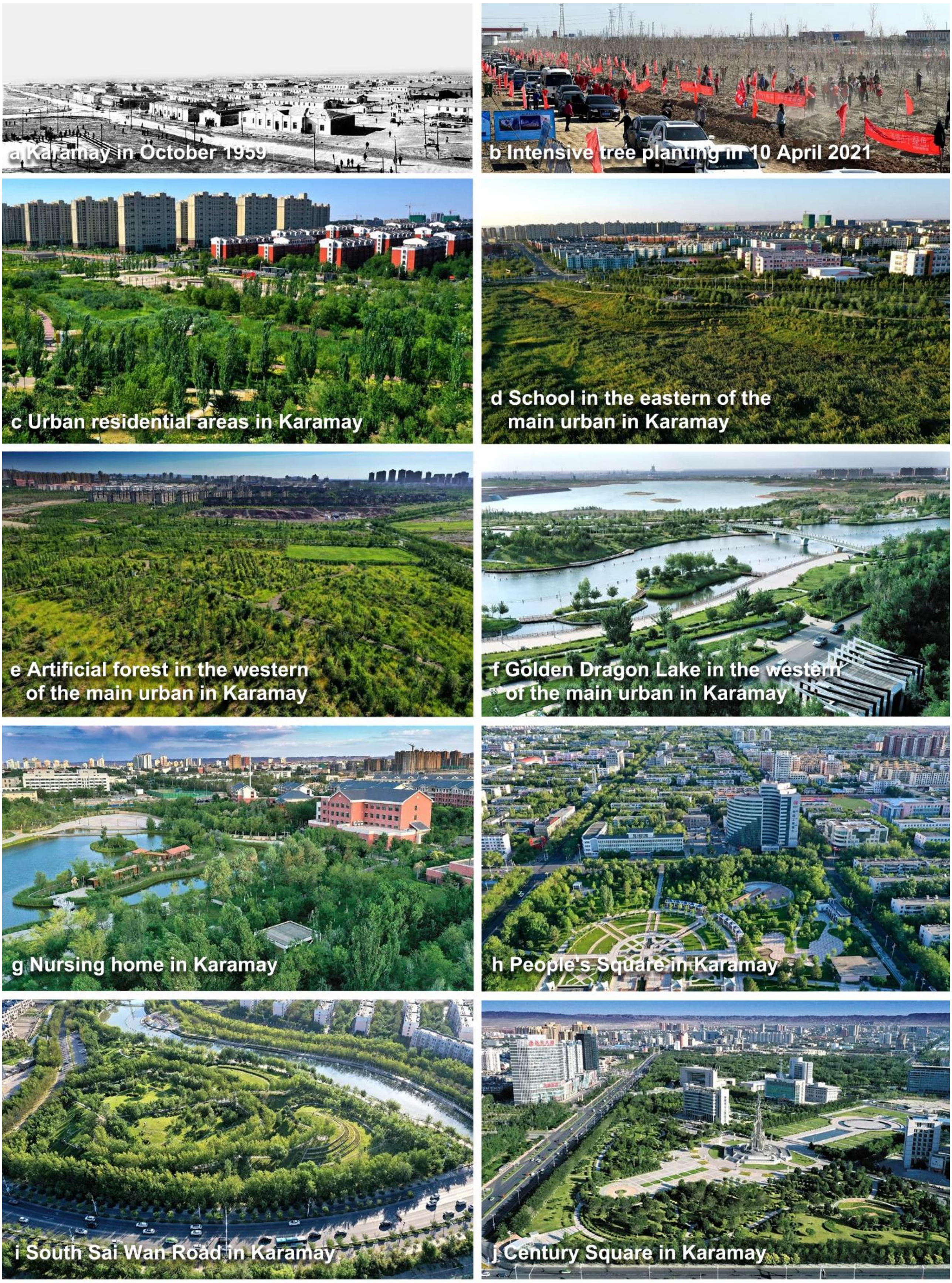

Supplementary Text Fig. 2 | The "greening" path in Karamay urban. The picture is from Karamay Newspaper (http://epaper.kelamayi.com.cn/).

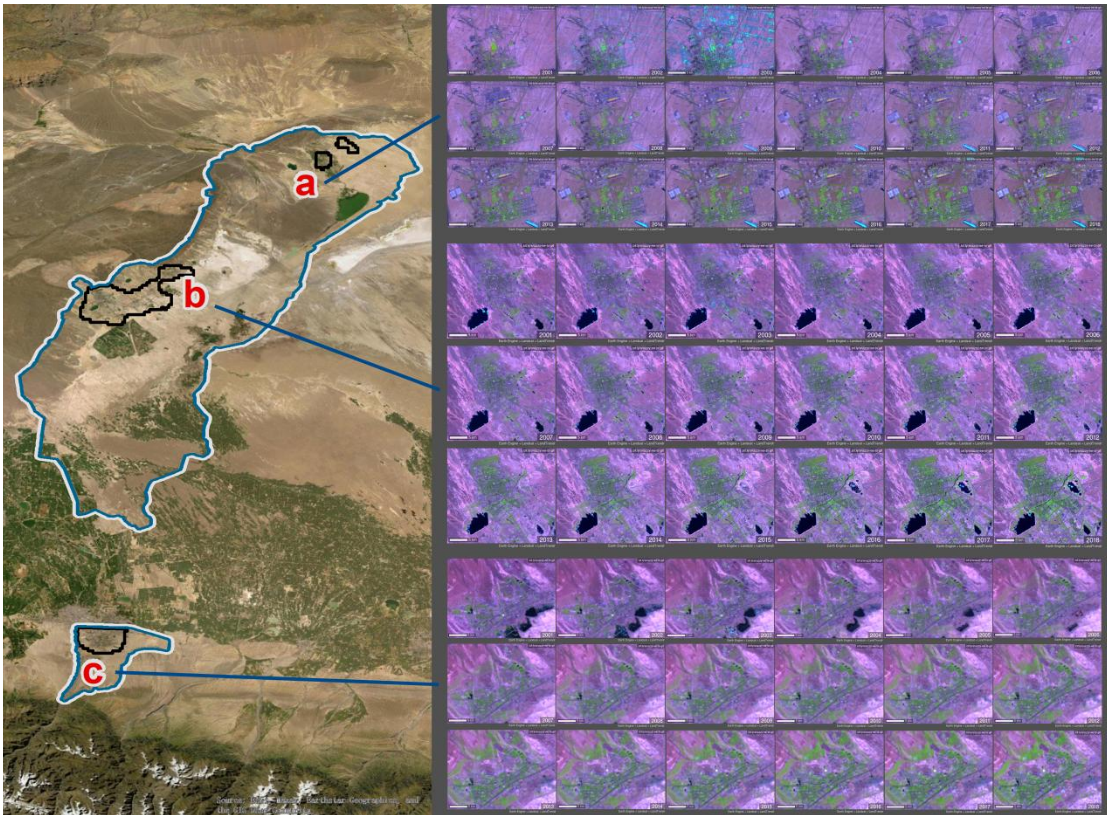

Supplementary Text Fig. 3 | False-color composite image of Landsat of three core urban areas in Karamay from 2001 to 2018 (R: SWIR1, G: NIR, B: RED). Greener pixels in the false-color composite image represent more vigorous vegetation growth.

Supplementary Text 3 | Inequality in the exposure of CPUG

We investigated the effects of economic, demographic, and social urbanization on the cooling potential of urban green spaces (CPUG) in China, similar to the effects of spatial urbanization [7]. At the provincial and 1000-m grid cell scales, we analyzed the relationship between CPUG and changes in urban GDP, urban electricity consumption (EC), urban carbon emissions (CE), and urban population (POP) from 2001 to 2018. Of the 24 provinces we studied, the largest CPUG was in Shaanxi (1.94 ± 1.48 K), followed by Gansu (1.90 ± 1.63 K) and Qinghai (1.68 ± 1.62 K), with a CPUG greater than 0. Those provinces that were exposed to CPUG added 522 million tons of CE, 747 billion kWh of EC, \$3.22 trillion (in 2017), and 54.10 million people over the last two decades (Supplementary Text Fig. 4). In contrast, the 9 provinces that were not exposed to CPUG added 679 million tons of CE, 877 billion kWh of EC, \$3.36 trillion (in 2017), and 50.4 million people (Supplementary Text Fig. 4). The focus of work in developing provinces remains on the construction of economic infrastructure due to their immature urbanization stage, while the CPUG will gradually emerge when the economic foundation can carry the superstructure [8].

There was a strong linear relationship between the GDP, *EC*, *CE* and POP in 2018 at the provincial scale (Supplementary Text Fig. 4e-g). However, the CPUG varied greatly among provinces. As the province with the second largest population, the CPUG in Jiangsu in the past two decades was only -1.32 ± 1.93 K, ranking last among all provinces. In 2018, Jiangsu consumed 280 billion kWh of EC (Supplementary Text Fig. 4b), accounting for 11.98% of China's total EC, emitted 158 million tons of CE (Supplementary Text Fig. 4c), accounting for 11.52% of China's total CE, and created a fiscal budget of \$0.98 trillion (in 2017) (Supplementary Text Fig. 4a), accounting for 10.95% of China's total GDP, which indicates that Jiangsu was in the stage of rapid development and may face major challenges for the urban ecological environment. In terms of the EC, CE, and GDP, Guangdong was second only to Jiangsu, but unlike Jiangsu Province, the CPUG of Guangdong Province was 0.57 ± 1.75 K. As the first province to set up special economic zones in the Reform and Opening Up and the province with the largest population, Guangdong has formed the Guangdong-Hong Kong-Macao Greater Bay Area with Hong Kong and Macau, becoming the world's leading manufacturing center, a major global innovation centre, and an international financial, shipping, and trade centre, which contributes 12.5% of China's GDP but only accounts for 1% of the land

[9]. This has also made Guangdong gradually develop into a new type of exo-urbanization in the course of nearly 40 years of development; that is, while developing the economy, it also pursued a high-quality living environment.

We examined the impact of CPUG on the GDP, EC, CE, and POP under static conditions in 2018. Our results indicate that over half of the total GDP (56.40%), total EC (54.68%), total CE (59.57%), and total POP (65.76%) were subjected to positive CPUG. Furthermore, we observed that the average GDP (Supplementary Text Fig. 4h), CE (Supplementary Text Fig. 4j), and POP (Supplementary Text Fig. 4k) of pixels exposed to the CPUG were higher than those of pixels not exposed to the CPUG, except for EC (Supplementary Text Fig. 4i). Supplementary Text Fig. 5 illustrates that areas with advanced levels of urbanization have a greater capacity to consume resources, release more greenhouse gases, and generate more GDP. This implies that the likelihood of CPUG exposure is greater in more developed urbanized areas. Thus, differences in the level of urbanization are the primary reason for the heterogeneity of CPUG in urban core-sprawl regions, which leads to a certain degree of social inequality in cities.

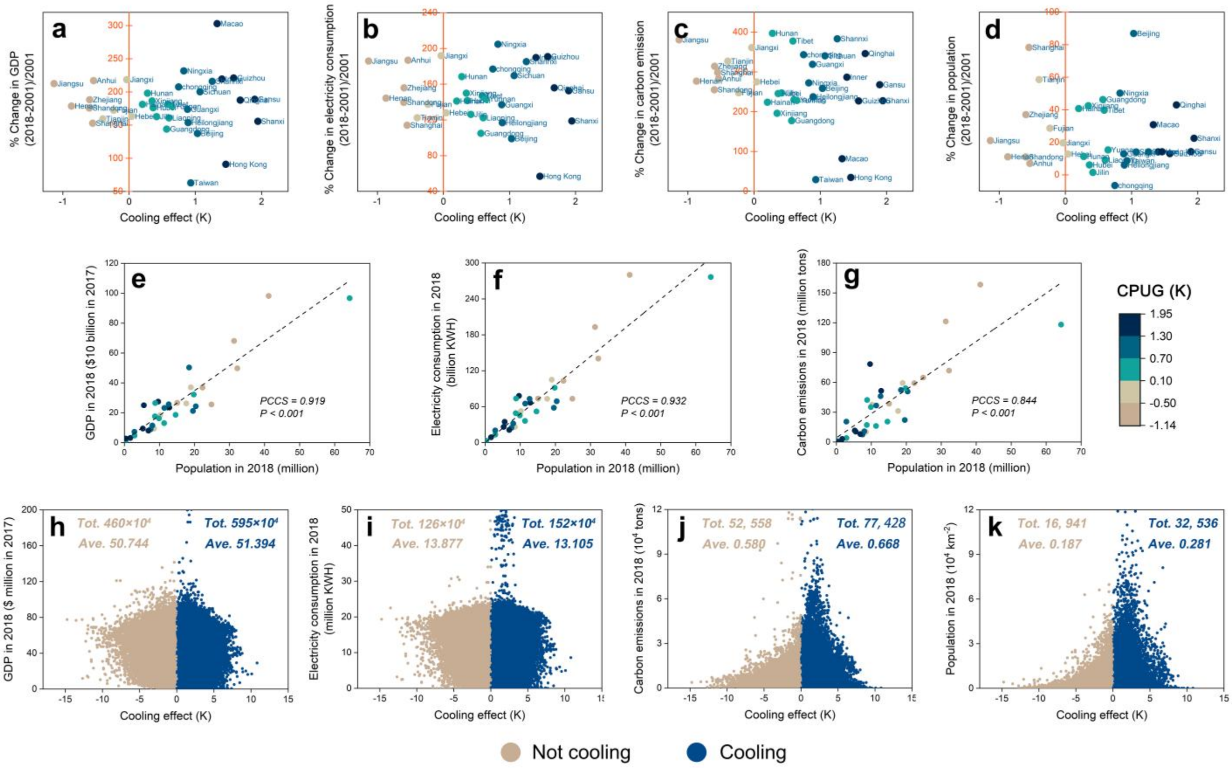

Supplementary Text Fig. 4 | Relationship between the GDP, electricity consumption (EC), carbon emissions (CE), population (POP), and CPUG. a, Relationship between the GDP change and the CPUG from 2001 to 2018 at the provincial scale. b, Relationship between EC changes and the CPUG from 2001 to 2018 at the provincial scale. c, Relationship between CE changes and the CPUG from 2001 to 2018 at the provincial scale. d, Relationship between the POP change and the CPUG from 2001 to 2018 at the provincial scale. e, Relationship between the GDP and POP at the provincial scale in 2018. f, Relationship between the EC and POP at the provincial scale in 2018. g, Relationship between the CE and POP at the provincial scale in 2018. h, Relationship between the GDP and the CPUG at the 1000-m grid cell scale in 2018. i, Relationship between the EC and the CPUG at the 1000-m grid cell scale in 2018. j, Relationship between the CE and the CPUG at the 1000-m grid cell scale in 2018. k, Relationship between the POP and the CPUG at the 1000-m grid cell scale in 2018.

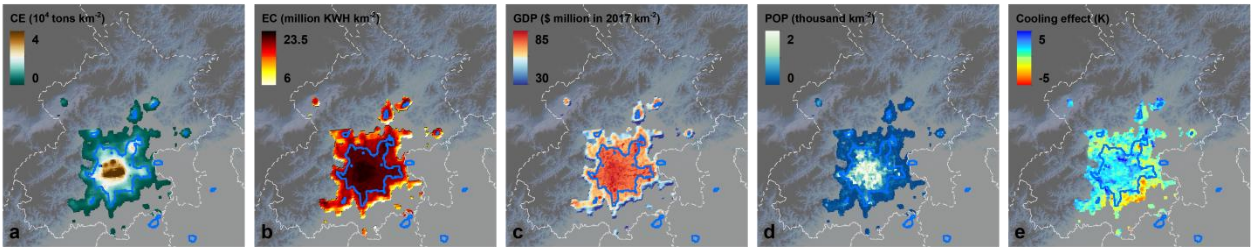

Supplementary Text Fig. 5 | Spatial distribution maps of carbon emissions (*CE*), electricity consumption (*EC*), GDP, and population density (POP) in Beijing in 2018 at 1000-m grid cell scale. a, Spatial distribution map of *CE* in 2018 at 1000-m grid cell scale. b, Spatial distribution map of *EC* in 2018 at 1000-m grid cell scale. *c,* Spatial distribution map of GDP in 2018 at 1000-m grid cell scale. d, Spatial distribution map of POP in 2018 at 1000-m grid cell scale. The blue polyline is the MUB.

Supplementary Text 4 | Evaluation of eco-environmental quality (EEQ)

On the basis of the original RSEI model [10], this study developed a new EEQ evaluation model for remote sensing data and produced China's high-resolution eco-environmental quality data.

This study developed a novel EEQ evaluation model for remote sensing data based on the original RSEI model [10]. And, this model was employed to generate China's high-resolution eco-environmental quality data (CHEQ).

$$CHEQ = \frac{PC1 - PC1_{\min}}{PC1 - PC1_{\max}} \tag{1}$$

$$PC1 = PCA(NDVI, NDBSI, LST, WET, AI) \tag{2}$$

where *CHEQ* is the EEQ index, *PC1* is the first principal component, $PC1_{min}$ is the minimum value of *PC1*, $PC1_{max}$ is the maximum value of *PC1*, and *NDVI*, *NDBSI*, *LST*, *WET*, and *AI* are the greenness, dryness, heat, humidity, and abundance index for the land cover type, respectively. NDVI and LST are MOD13A2 and MOD11A1 products, respectively, and both NDBSI and WET are calculated based on the MOD09A1 [10].

The RSEI model is a conventional tool used to monitor the EEQ at the local level. Despite some scholars [11] having employed the RSEI model to assess China's EEQ, only a limited number have explored its applicability in the country. Hence, we have improved the RSEI model and evaluated the applicability of the RSEI and CHEQ in China.

Specifically, the ecological index calculation greatly depended on the abundance index of land cover types (*AI*), while four of the aforementioned indices in the RSEI model did not involve the important evaluation factor. Therefore, after referring to the "Technical Criterion for Ecosystem Status Evaluation [12], we calculated the *AI* in the study area during 2001-2018 based on the MCD12Q1 data. The *AI* was calculated as follows:

The ecological index calculation heavily relies on the Abundance Index (AI) of land cover types. However, four indices in the RSEI model fail to account for this crucial evaluation factor. To address this issue, we consulted the "Technical Criterion for Ecosystem Status Evaluation" [12] and calculated the AI for the study area between 2001-2018, using MCD12Q1 data. The AI was calculated using the following formula:

$$\begin{aligned} AI = \mu \times (&0.35 \times Forest + 0.21 \times Grassland + 0.28 \times Water + \\ &0.11 \times Cropland + 0.04 \times Built + 0.01 \times Unused) / Area \end{aligned} \tag{3}$$

where *AI* is the abundance index for land cover types, μ is the normalized coefficient, *Forest*, *Grassland*, *Water*, *Cropland*, *Built*, and *Unused* are the areas of forestland, grassland, waterbody, cropland, built-up, and unused land, respectively, and *Area* is the total area.

Supplementary Text 5 | Potential impact of ecological restoration projects (ERPs) on CEUG

In this study, we gathered data on the primary ERPs in China (see Supplementary Table 1), evaluated their pilot regions, and subsequently categorized China into four ERP regions and one Non-ERP region (Supplementary Text Fig. 6).

We improved upon the research conducted by Xu et al. [1] by creating the China High-Resolution Eco-Environmental Quality dataset (CHEQ) for 2001-2018 (see Supplementary Text 2 for calculation details). Additionally, we gathered 2,334 ecological index (EI) data at the county level throughout China to verify the accuracy of the eco-environmental quality (EEQ) data before and after our improvements (Extended Data Fig. 9). Compared to the traditional RSEI, our study's CHEQ data demonstrate greater universality across various districts of China. Urban clusters with rising EEQ in China were mainly situated in northern, southwestern, and coastal regions, while urban EEQ in the North China Plain and the middle and lower reaches of the Yangtze River Plain showed a declining trend (Extended Data Fig. 10) in the past two decades. This finding is consistent with the spatial distribution of Sen_NDVI (Fig. 2i). As CHEQ increases, the CPUG becomes more pronounced. The mean CPUG of all urban clusters categorized as E1 is -0.21 ± 1.50 K, whereas the mean CPUG of all urban clusters categorized as E5 is 1.45 ± 1.47 K (Extended Data Fig. 10c). Furthermore, 64.18% of urban clusters categorized as E5 have a CPUG greater than 0, compared to only 7.48% of urban clusters categorized as E1 (Extended Data Fig. 10c).

From the perspective of ERPs, we observed that most urban clusters in the Beijing-Tianjin Sandstorm Source Control Project (BTSSCP) and the 3-North Shelter Forest Program (3-NSFP) effectively cooled the urban land surface, with 92.96% and 78.57% of urban clusters having a CPUG greater than 0, respectively (Extended Data Fig. 10d). For the Coastal Shelter Forest Project (CSFP) and Other ERP, the proportions were 69.79% and 61.61%, respectively. In contrast, urban clusters in the Non-ERP area had the smallest proportion, which was only 20.48% (Supplementary Text Fig. 7b and 7d). The BTSSCP had the largest CPUG (1.20 ± 1.57 K) among all ERPs, followed by the 3-NSFP (0.77 ± 1.95 K), Other ERP (0.30 ± 2.02 K), and CSFP (0.17 ± 1.91 K). In comparison, urban clusters in the Non-ERP area had the smallest CPUG, which was only -0.87 ± 1.83 K (see Supplementary Text Fig. 7).

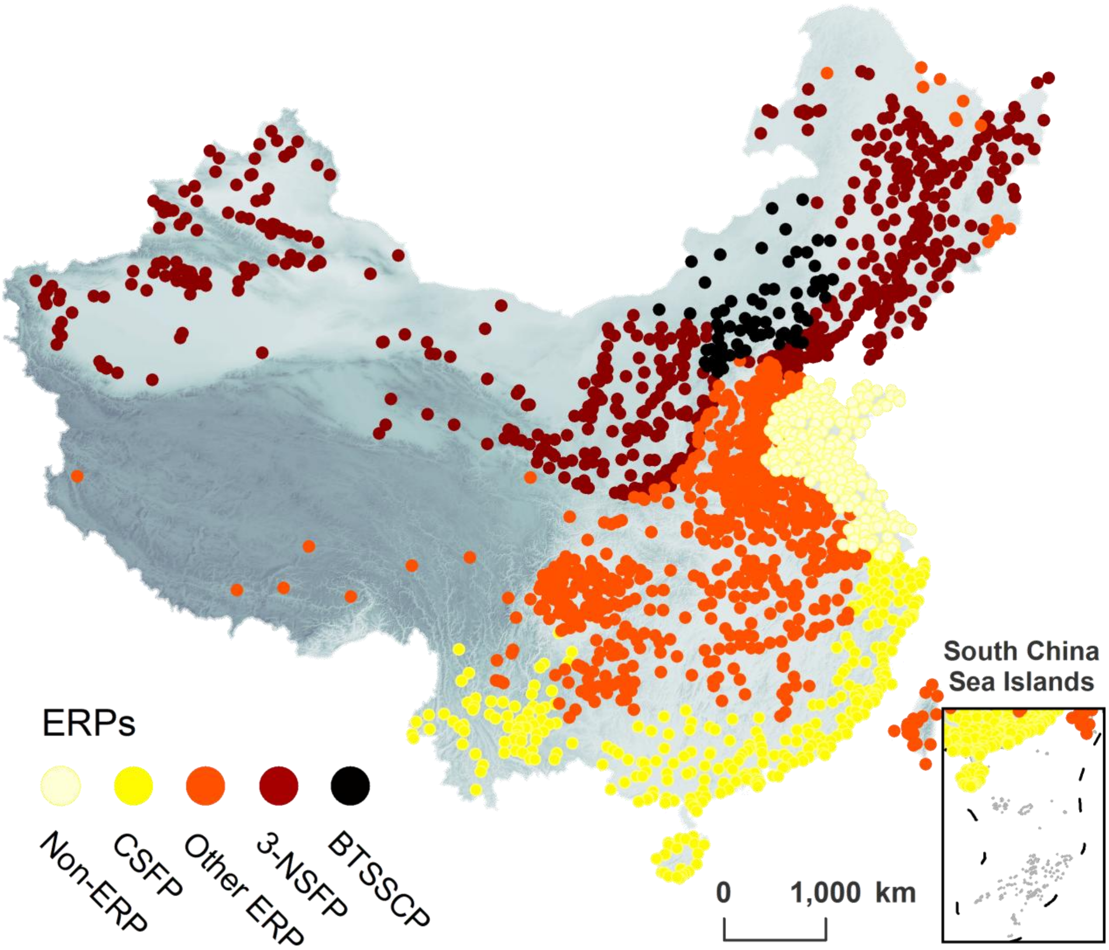

Supplementary Text Fig. 6 | Spatial distribution map of urban clusters classification according to ERPs. BTSSCP is the abbreviation for Beijing-Tianjin Sandstorm Source Control Project. 3-NSFP is the abbreviation including 3-North Shelter Forest Program, Natural Forest Protection project, Reclainled Frmland to Forest project, Reclainled Pasture to Grass, Ecological Protection and Construction of Sanjiangyuan Nature Reserve, National Nature Reserve, among which 3-North Shelter Forest Program is the main ERP. Other ERP is the abbreviation including Reclainled Frmland to Forest project, Shelter Forest System in the Yangtze River Basin, Taihang Mountain Greening Project，Plain Greening Project，National Wetland Protection Project，Reclainled Farmland to Lake and National Nature Reserve. CSFP is the abbreviation for Coastal Shelter Forest System Project and Coastal Shelter Forest Project. Non-ERP is the abbreviation for Shandong and Jiangsu.

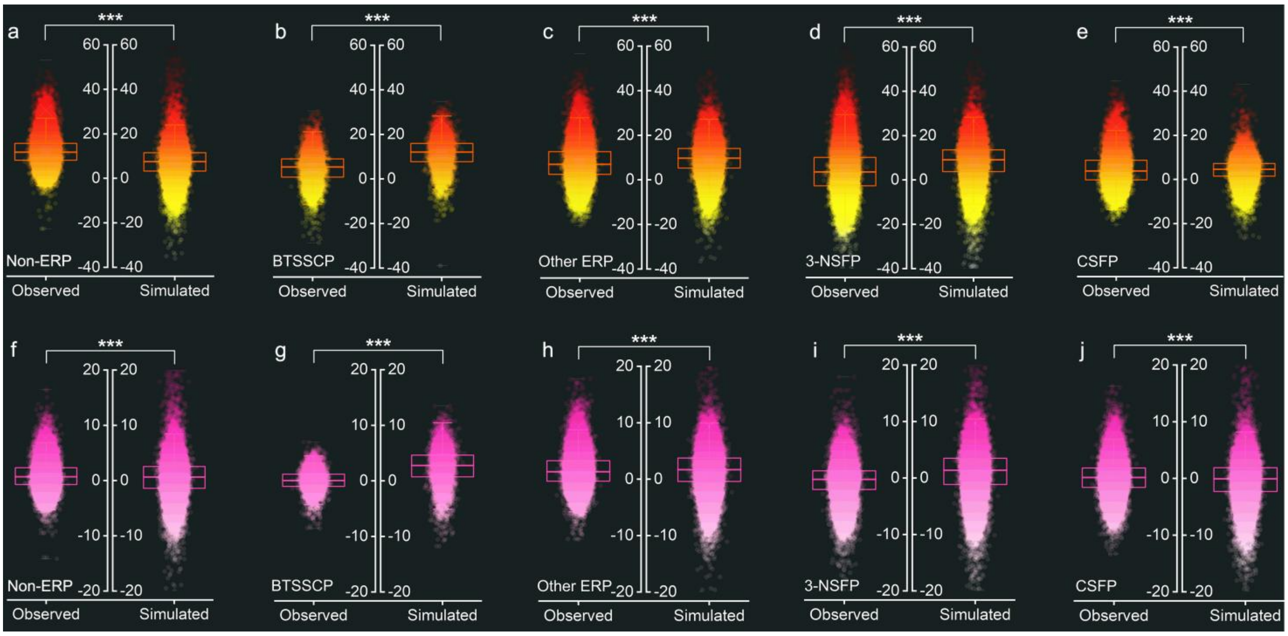

Supplementary Text Fig. 7 | Numerical distribution diagrams of Sen_UST (observed, simulated) and Sen_IBI (observed, simulated) of different ERPs partitions. a, Observed and simulated Sen_UST in Non-ERP. b, Observed and simulated Sen_UST in BTSSCP. c, Observed and simulated Sen_UST in Other ERP. d, Observed and simulated Sen_UST in 3-NSFP. e, Observed and simulated Sen_UST in CSFP. f, Observed and simulated Sen_IBI in Non-ERP. g, Observed and simulated Sen_IBI in BTSSCP. h, Observed and simulated Sen_IBI in Other ERP. i, Observed and simulated Sen_IBI in 3-NSFP. j, Observed and simulated Sen_IBI in CSFP. '***' represents a significant difference between the two groups of samples at least at the 1% level.

In the four ERPs, UG showed an overall upwards trend in the past two decades (Supplementary Text Fig. 8a-e). Similar to the CPUG, the growth rate of UG in the BTSSCP was the largest (22.04%), followed by 3-NSFP (18.12%), Other ERP (1.11%), and CSFP (0.12%), and UG in the non-ERP partition showed a downwards trend (-2.47%). Among the five CPUG levels (C1-C5), the overall UG growth rate of the urban clusters at the C5 level was the largest, while the overall UG decline rate of the urban clusters at the C1 level was the largest (Supplementary Text Fig. 8). In the 3-NSFP, BTSSCP, Other ERP, and CSFP, the UG growth rates of the C5-level urban clusters were 56.85%, 33.94%, 15.82%, and 7.87%, respectively, while the UG decline rates of the C1-level urban clusters were -1.02% (3-NSFP), -7.51% (Other ERP), -16.24% (CSFP), and -11.92% (Non-ERP). On the other hand, the UI showed an overall upwards trend in the Non-ERP (34.68%), CSFP (10.77%), and Other ERP (32.11%) partitions, while the UI in the 3-NSFP (-143.44%) and BTSSCP (-3.78) showed a downwards trend (Supplementary Text Fig. 8f-j). The UI of the C5-level urban clusters had the largest decline rate, while the UI of the C1-level urban clusters had the largest growth rate. In the 3-NSFP, Other ERP, CSFP, and Non-ERP partitions, the UI growth rates of the C1-level urban clusters were

0.83%, 0.97%, 1.30%, and 0.97%, respectively, while the UI decline rates of the C5-level urban clusters were -0.30% (3-NSFP), -0.07% (Other ERP), -0.20% (CSFP), and -0.30% (BTSSCP). A series of ERPs have made China the country with the largest planted forest area in the world [13,14], accounting for approximately 25% of the global planted forest area [15]. Through this study, we found that ERPs can not only promote forest vegetation greening but also effectively cool urban land surfaces.

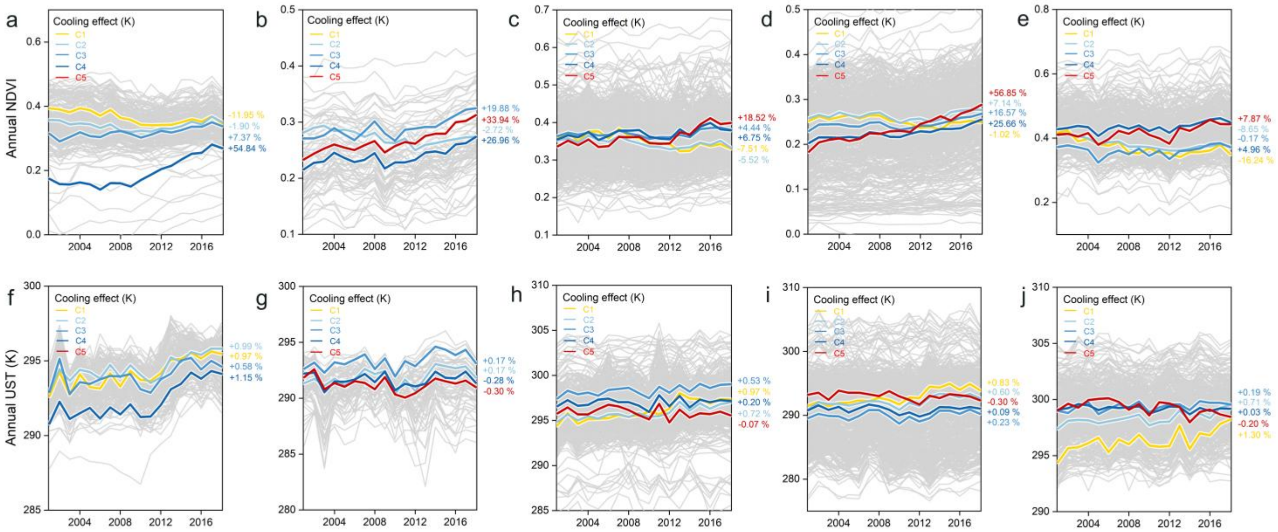

Supplementary Text Fig. 8 | Annual NDVI and UST time series maps (at the cluster scale and different gradients of CPUG) in different ERP partitions. a, Annual NDVI time series in the Non-ERP. b, Annual NDVI time series in the BTSSCP. c, Annual NDVI time series in Other ERP. d, Annual NDVI time series in the 3-NSFP. e, Annual NDVI time series in the CSFP. f, Annual UST time series in Non-ERP. g, Annual UST time series in the BTSSCP. h, Annual UST time series in Other ERP. i, Annual UST time series in the 3-NSFP. j, Annual UST time series in the CSFP.

Supplementary Figure (1-9)

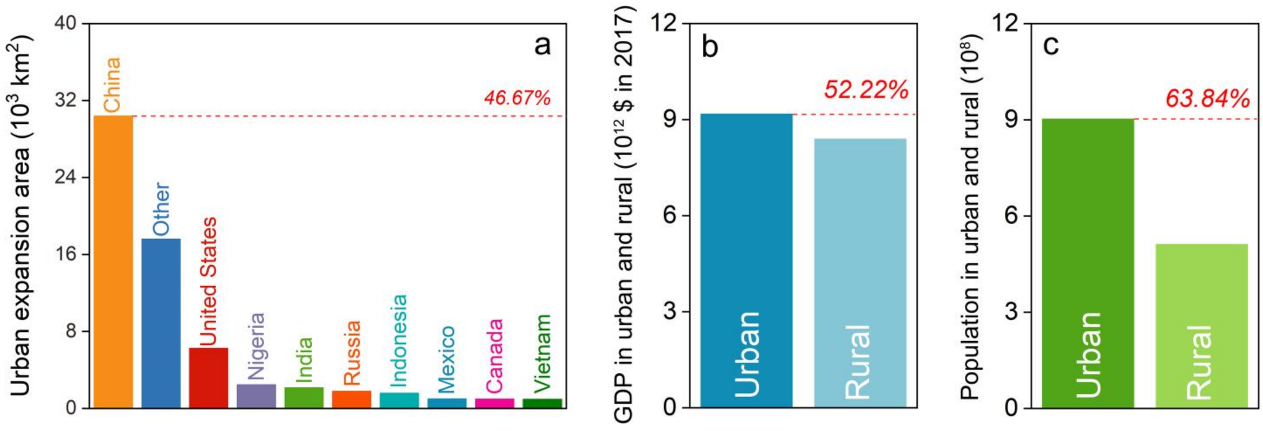

Supplementary Fig. 1 | Global urban expansion area during 2001-2018 and population, GDP status in China. a, Urban expansion in major countries worldwide during 2001-2018. b, China's urban-rural GDP difference in 2018. c, China's urban-rural population difference in 2018. Urban and rural data from the Global Urban Boundaries dataset [14]. The population data from Worldpop (http://www.stats.gov.cn/). The GDP data from the study by Chen et al [15].

In the past two decades, China's rapid and high-quality urbanization [9] has led to significant greening in some large cities (see the spatial distribution map of Sen_NDVI in Supplementary Fig. 2a), primarily due to increases in green infrastructure such as parks and green spaces [2]. Moreover, UG has significantly cooled these cities (see the Sen_UST spatial distribution map in Supplementary Fig. 2b). However, despite these efforts, the increase in UG led by large cities (as shown in the NDVI time series curve in Supplementary Fig. 2a) has been insufficient to restrain the urban warming trend caused by UG degradation in small and medium-sized cities (as shown in the UST time series curve in Supplementary Fig. 2b) [16]. Thus, information regarding the quantity and quality of the CPUG in China in the past 20 years is crucial for mitigating the global urban heat wave.

We excluded areas with less human activities, such as suburbs and rural areas [17], by mapping the largest urban boundaries (LUB) based on Global Urban Boundaries data [18] in China from 2001 to 2018. These areas were considered as the study areas in this research. The study areas are situated in the South Asia tropical (SS), central Asian tropical (MS), north subtropical (NS), warm temperate (WT) and middle temperate (MT) zones [19]. They are primarily located in the eastern and southeastern coastal regions with flat terrain, while a few are distributed in the Chengdu Plain and other inland areas (Supplementary Fig. 2). The total area of the study areas is about 17.83 million km^2, which accounts for approximately 1.86% of China's land area.

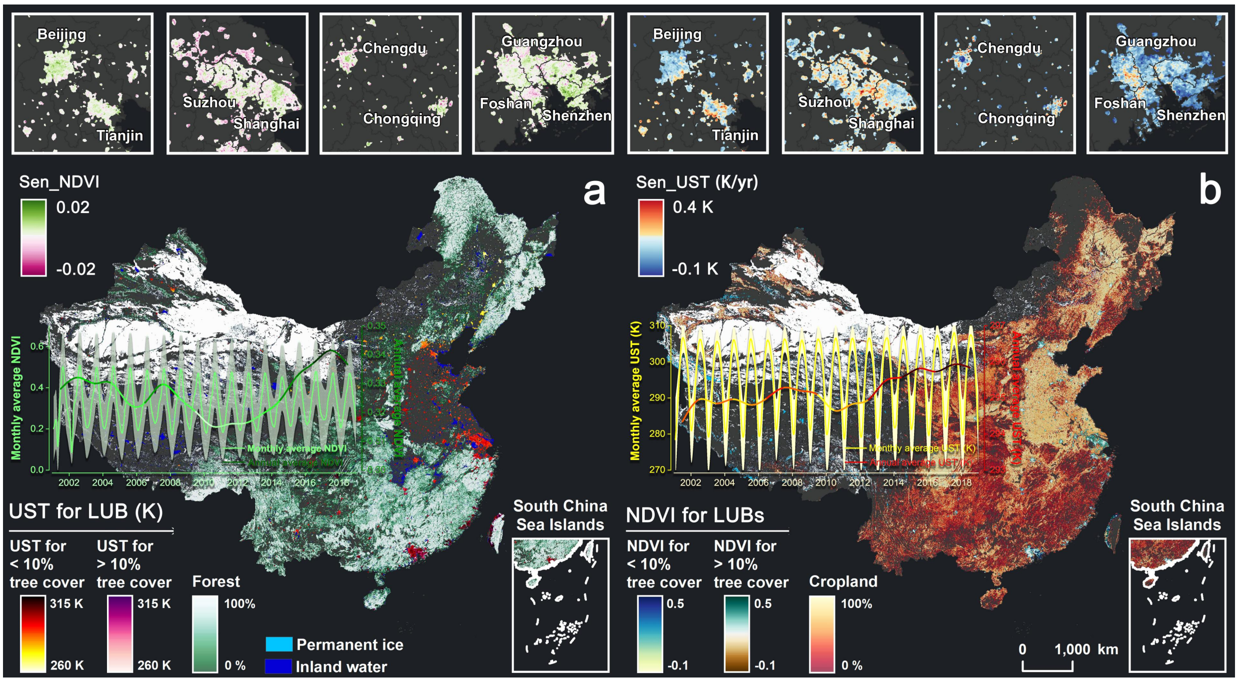

Supplementary Fig. 2 | Spatial distribution map of LUB, ecosystem type patterns, Sen_NDVI, Sen_UST, and UST and NDVI time series of LUB from 2001 to 2018 in China. a, UST for LUB in 2018 with tree cover below 10% and above 10%. The green curve with confidence interval (standard deviation) is the monthly variation process of NDVI for LUB from 2001 to 2018. The curve of gradient color is the annual variation process of NDVI for LUB from 2001 to 2018. The top four maps are the Sen_NDVI distribution map of China's four major urban agglomerations (Beijing-Tianjin-Hebei, Yangtze River Delta, Chengdu-Chongqing, and Pearl River Delta) from 2001 to 2018. b, NDVI for LUB in 2018 with tree cover below 10% and above 10%. The yellow curve with confidence interval (standard deviation) is the monthly variation process of LST for LUB from 2001 to 2018. The curve of gradient color is the annual variation process of LST for LUB from 2001 to 2018. The top four maps are the Sen_UST distribution map of China's four major urban agglomerations (Beijing-Tianjin-Hebei, Yangtze River Delta, Chengdu-Chongqing, and Pearl River Delta) from 2001 to 2018. Tree cover data comes from GFCC data [20] in 2015. The green and orange legends respectively represent the forest cover rate and cropland and cover rate in China, and the data come from CLUDs [21] data in 2015.

The results of the universality test of the CPUG model are presented in Supplementary Fig. 3. The figure shows that the human activity parameter accounts for 81% of the pixels and 86% of the urban clusters, indicating that human activities have been the primary driver of UST variations in urban areas in China in the past two decades. This finding is consistent with the conclusion in the handbook [22], which suggests that the mutual transformation of urban green space and impervious surfaces is the main form of human activity. The IBI and NDVI are the most sensitive indicators, supporting the handbook's findings and demonstrating the CPUG model's universality in China's urban areas.

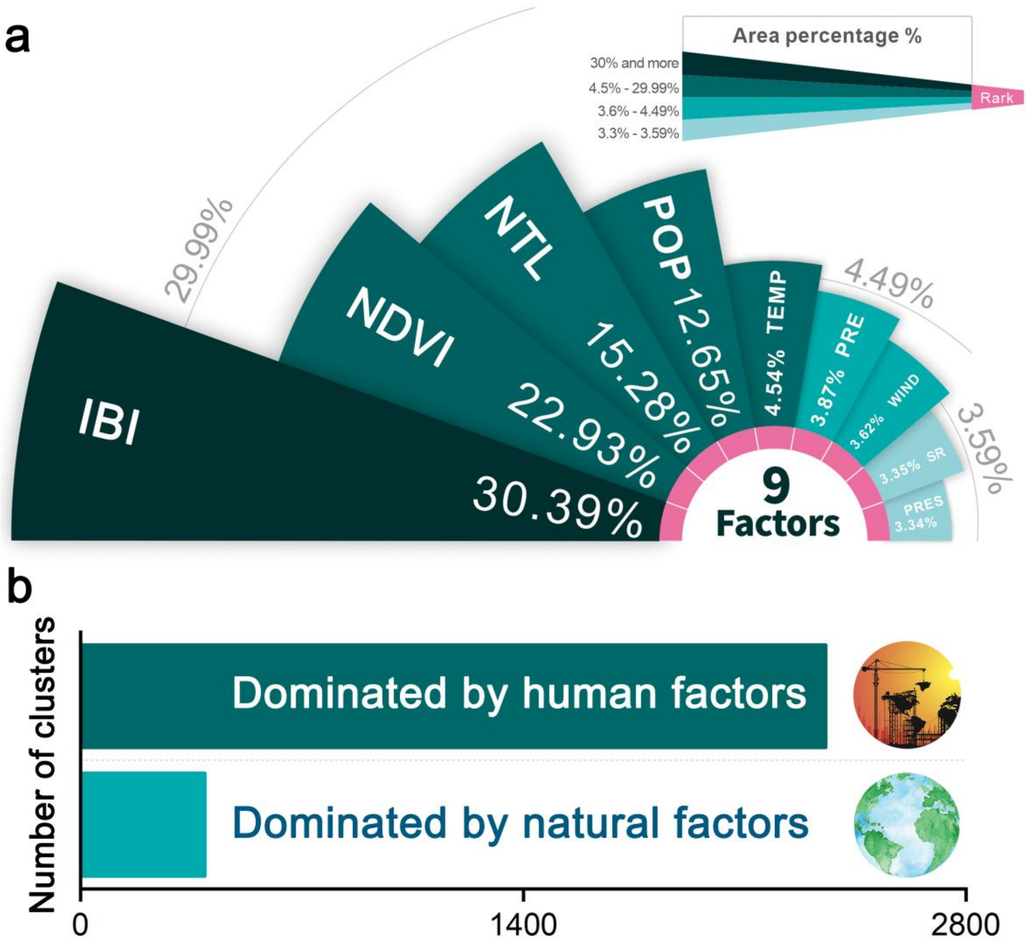

Supplementary Fig. 3 | Sensitivity analysis results of UST in the observation dimension of the system time series at the 1000-m grid cell scale. a, UST pixel ratio driven by different influencing factors. b, Number of urban clusters driven by human (IBI, NDVI, NTL and POP) and natural factors (TEMP, PRE, WIND, *SR* and PRES).

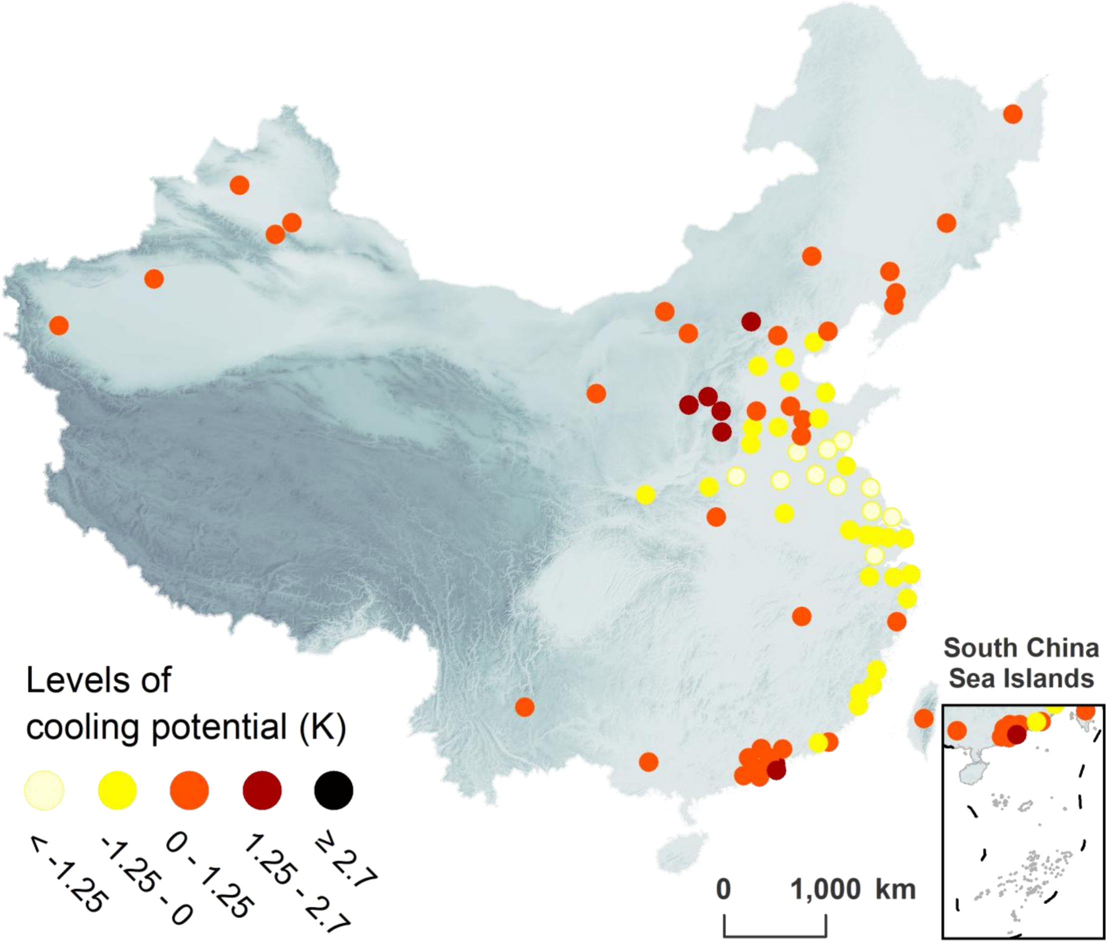

Supplementary Fig. 4 | Spatial distribution map of CPUG in 79 cities with urban area greater than 500 km^2. Each point is the center of gravity of the administrative boundary of each city, not the center of gravity of the urban.

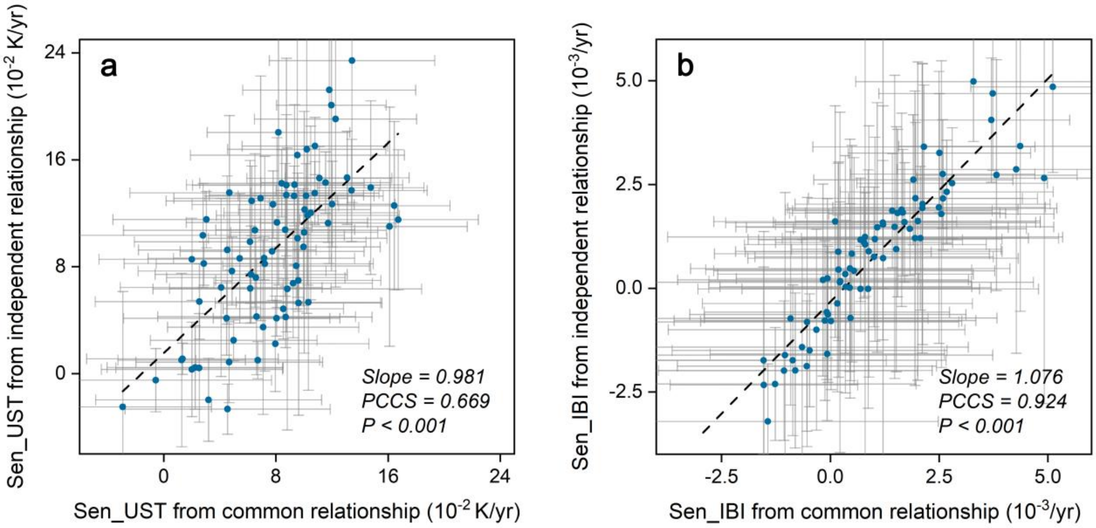

Supplementary Fig. 5 | Accuracy verification of Sen_UST, Sen_IBI simulated by 79 independent empirical relationships and those simulated by common relationship of China. a, Accuracy verification of Sen_UST. b, Accuracy verification of Sen_IBI.

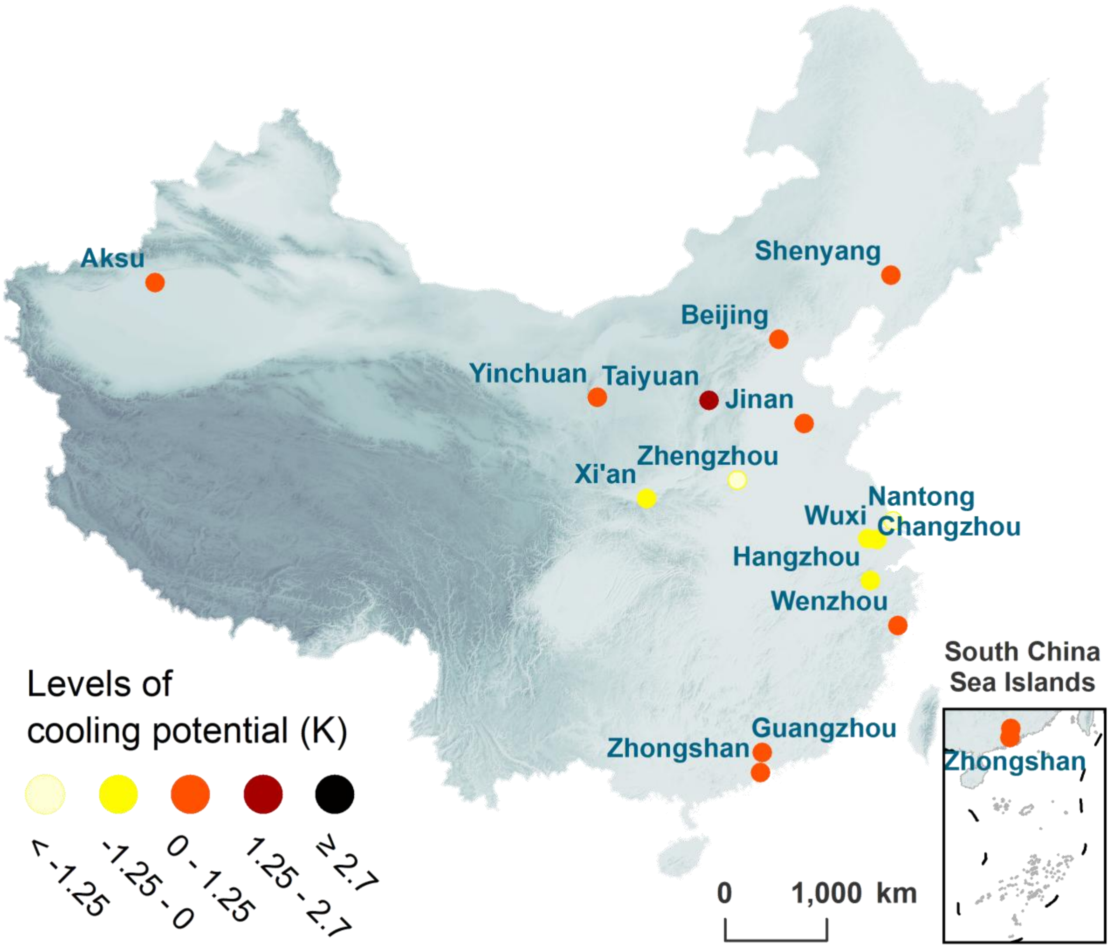

Supplementary Fig. 6 | Spatial distribution map of UG cooling potential in 15 typical cities. Each point is the center of gravity of the administrative boundary of each city, not the center of gravity of the urban.

The environmental Kuznets curve (EKC) [23] holds that when urbanization reaches the highest stage, the urban ecological environment will improve as the urbanization level increases. With the process of urbanization, the proportion of the urban population will continue to rise, which leads to a more significant demand for the urban living environment. Taking Beijing as an example, the urbanization rate reached 80% and has been stable at 80-87%, which means that the urbanization of Beijing in the past two decades has reached a saturation stage. Correspondingly, living standards are also improving, and the demand for a high-quality living environment is becoming increasingly urgent. The high-resolution satellite imagery also directly confirms our conclusion (Supplementary Fig. 7).

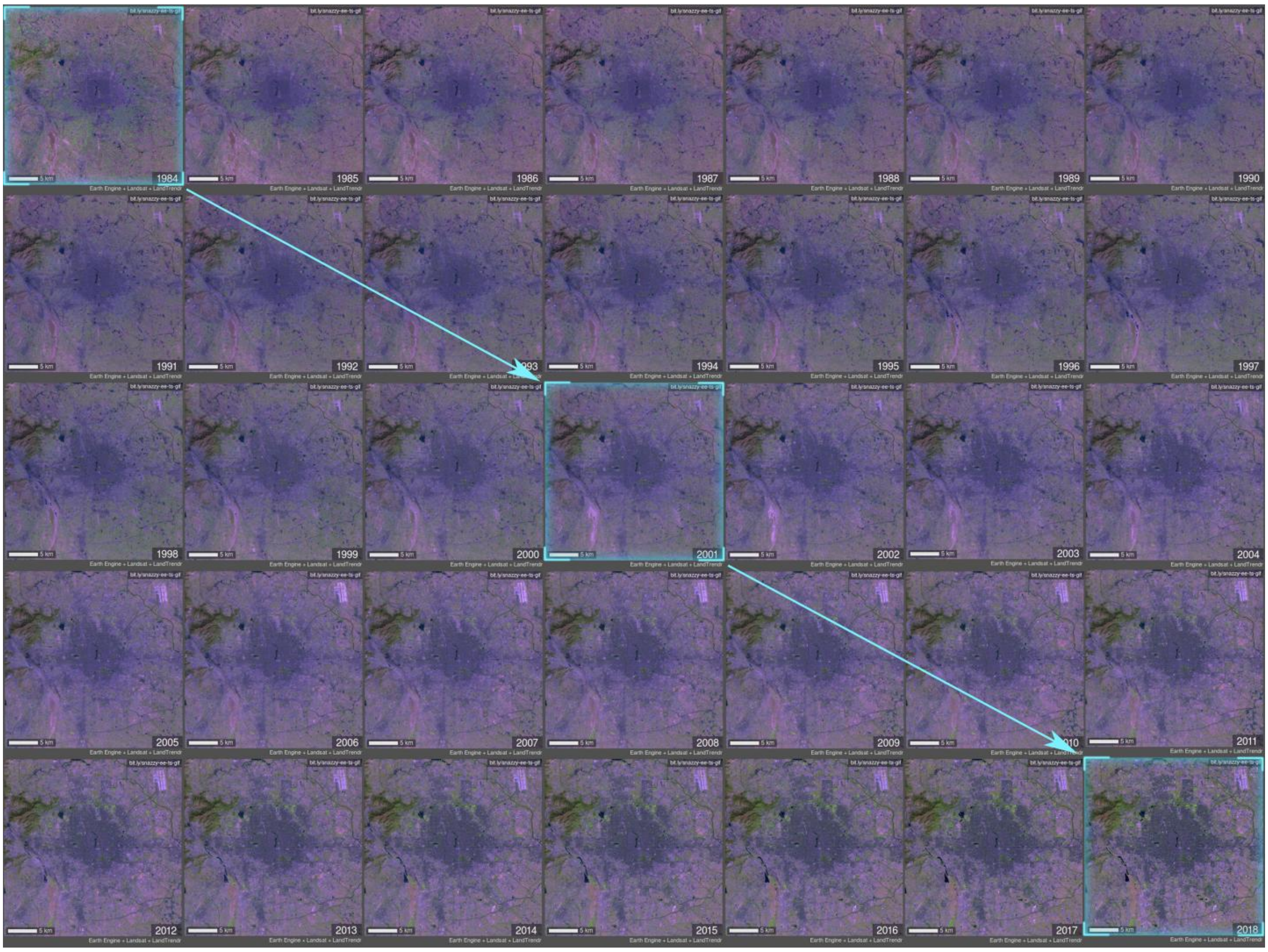

Supplementary Fig. 7 | False-color composite image of Landsat of urban areas in Beijing from 1984 to 2018 (R: SWIR1, G: NIR, B: RED). Greener pixels in the false-color composite image represent more vigorous vegetation growth.

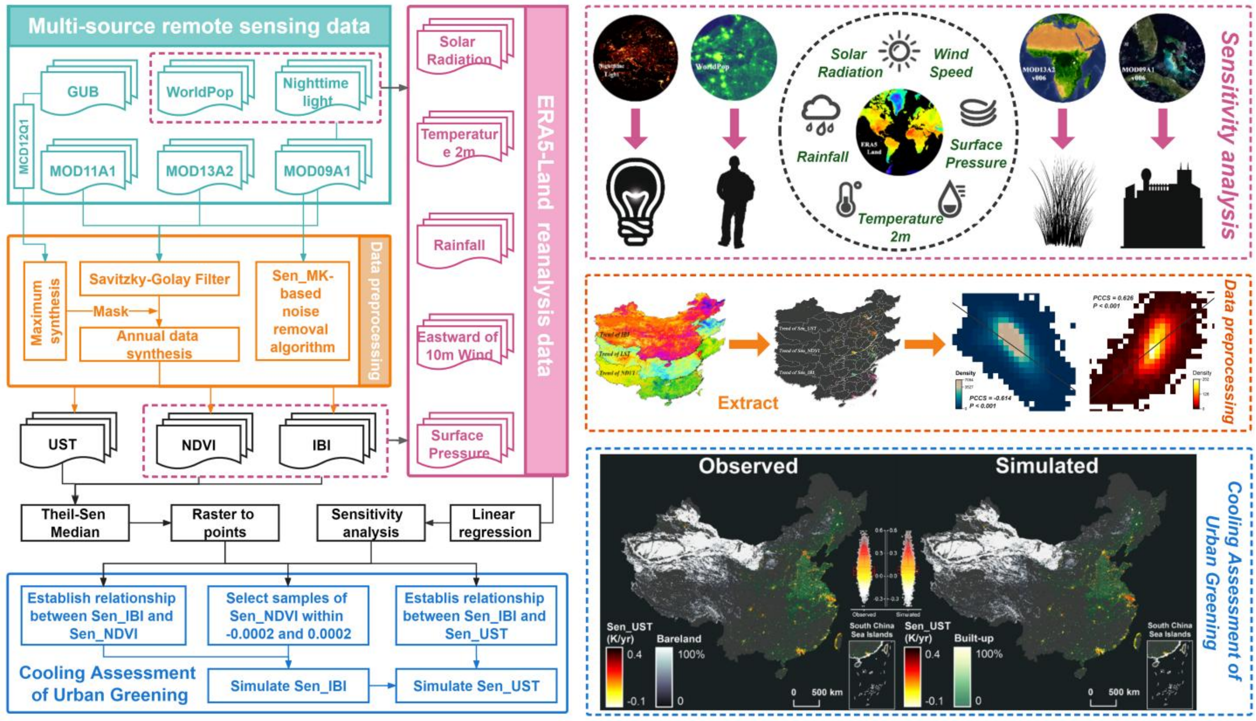

a. Flowchart of the methodology. b. Conceptual diagram of the methodology.

Supplementary Fig. 8 | Method flowchart and conceptual diagram of quantitative CPUG from systematic time series observations. a, Flowchart of the methodology. The remote sensing data (green font) used to quantify the CPUG include Global Urban Boundaries, population density data, nighttime light data, daytime land surface temperature data (MOD11A1), normalized difference vegetation index (MOD13A2), and land surface reflectance data (MOD09A1). The reanalysis data is from the ERA5-land reanalysis data (pink font), and we selected solar radiation (short wave downward radiation), 2 m temperature, precipitation, 10 m wind speed (eartward), and surface pressure parameters as independent variables for the sensitivity analysis of UST (black font). The orange font part is the data preprocessing, which mainly includes the synthesis of the LUB, the smoothing (SG filter) of the annual index (UST, NDVI and IBI), and the denoising of nighttime light data. The blue font part is the CAUG framework, which consists of three steps. First, a linear statistical relationship between Sen_IBI and Sen_NDVI was constructed. Second, the linear statistical relationship between Sen_IBI and Sen_UST under the no-*UG* scenario (that is, pixels whose Sen_NDVI is between -0.0002 and 0.0002) is constructed. Finally, based on the two statistical relationships of step 1 and step 2, the Sen_UST under the no-*UG* scenario was simulated. b, Conceptual diagram of the methodology.

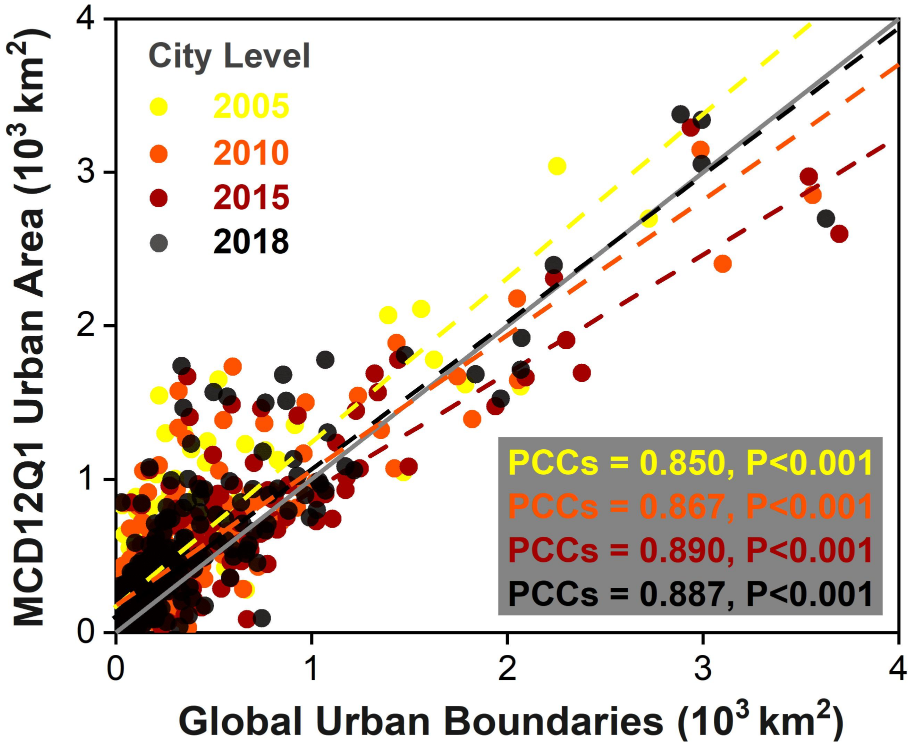

Supplementary Fig. 9 | Consistency detection between MCD12Q1 urban data and Global Urban Boundaries data in 2005, 2010, 2015 and 2018. In this study, the pixel with the MCD12Q1 data value of 13 was defined as the Urban area. The unit of each validation sample is the city level.

Graphic abstract

Graphic abstract| ∇T is the cooling factor of UG. The upper left graph shows the observed and simulated UST trends during 2001-2018. The gradient line in the middle represents the size of the UST. In the middle of the figure, the urban impermeability is high, so the gradient line is a red bulge state.

Supplementary Table (1-4)

Supplementary Table 1 | Ecological Restoration Projects in China.

Restore object	ERPs	Period	Pilot area	Investment (billion CNY
Forest	Natural Forest Protection project	1998-2010	Yunnan, Sichuan, Chongqing, Guizhou, Hunan, Hubei, Jiangxi, Shanxi, Shannxi, Gansu, Qinghai, Ningxia, Xinjiang, Inner Mongolia, Jilin, Heilongjiang, Hainan, Henan	962.02
	Reclainled Frmland to Forest project	1999-2021	Gansu, Inner Mongolia, Guizhou, Shanxi, Shannxi, Hunan, Hubei, Sichuan, Chongqing, Yunnan	4311.30
	3-North Shelter Forest Program	2001-2010	Xinjiang, Qinghai, Gansu, Ningxia, Inner Mongolia, Shannxi, Shanxi, Hebei, Liaoning, Jilin, Heilongjiang, Beijing, Tianjin	354.12
	Shelter Forest System in the Yangtze River Basin	2001-2010	Jiangxi, Hubei, Hunan, Sichuan, Guizhou, Yunnan, Shannxi, Gansu, Qinghai	205.61
	Beijing-Tianjin Sandstorm Source Control Project	2001-2010	Beijing, Tianjin, Hebei, Shanxi, Inner Mongolia	558.65
	Coastal Shelter Forest System Project	2001-2010	Liaoning, Heibei, Zhejiang, Fujian, Guangdong, Hainan, Guangxi	39.09
	Taihang Mountain Greening Project	2001-2010	Shanxi, Hebei, Henan, Beijing	35.97
	Plain Greening Project	2001-2010	More than 900 plains in China	12.47
	Coastal Shelter Forest Project	2006-2015	Liaoning, Heibei, Zhejiang, Fujian, Guangdong, Hainan, Guangxi	99.84
Wetland	National Wetland Protection Project	2005-2010	473 wetlands in China	90.04
	Reclainled Farmland to Lake	1998-2005	Cover the whole country	—
Grassland	Reclainled Pasture to Grass	2003-2007	Xinjiang, Xizang, Inner Mongolia, Qianghai, Gansu, Ningxia	143.00
Important ecological functions	Ecological Protection and Construction of Sanjiangyuan Nature Reserve	2005-2010	Qinghai	75.00
	National Nature Reserve	1999-2010	Cover the whole country	4.80

Supplementary Table 2 | Criteria for classifying Sen_UST, Sen_IBI and Sen_NDVI.

Range of Sen_UST	Level	Range of Sen_IBI	Level	Range of Sen_NDVI	Level
[-0.288, 0.040)	U1	[-0.009, -0.003)	B1	[-0.012, -0.003)	N1
[-0.040, 0.000)	U2	[-0.003, 0.000)	B2	[-0.003, 0.000)	N2
[0.000, 0.080)	U3	[0.000, 0.001)	B3	[0.000, 0.002)	N3
[0.080, 0.150)	U4	[0.001, 0.003)	B4	[0.002, 0.005)	N4
[0.150, 0.388)	U5	[0.003, 0.007)	B5	[0.005, 0.015)	N5

Supplementary Table 3 | Simulation results of CPUG in major cities.											
City	Sen_UST	Sen_IBI	Sen_NDVI	Simulated Sen_UST	Cooling effect	City	Sen_UST	Sen_IBI	Sen_NDVI	Simulated Sen_UST	Cooling effect
Aksu Area	0.0400	0.0015	0.0015	0.1058	1.1844	Lvliang	0.0248	0.0033	0.0041	0.1152	1.6268
Anshan	0.0959	0.0049	0.0020	0.2122	2.0934	Nanchang	0.0706	0.0008	-0.0009	0.0634	-0.1292
Anyang	0.1570	0.0027	-0.0009	0.1462	-0.1949	Nanjing	0.0730	0.0002	-0.0002	0.0719	-0.0198
Baoding	0.1582	0.0028	-0.0008	0.1429	-0.2746	Nanning	-0.0100	-0.0001	-0.0017	-0.0265	-0.2971
Baotou	0.0610	0.0026	0.0016	0.0948	0.6081	Nantong	0.1430	0.0009	-0.0034	0.0986	-0.7992
Beijing	0.0766	0.0022	0.0032	0.1371	1.0885	Nanyang	0.0752	0.0012	0.0010	0.0806	0.0973
Cangzhou	0.1105	0.0021	0.0006	0.1203	0.1765	Ningbo	0.1155	0.0002	-0.0017	0.0863	-0.5268
Changji	0.1334	0.0044	0.0018	0.2342	1.8138	Putian	0.0296	-0.0011	-0.0024	0.0032	-0.4742
Changzhi	0.0780	0.0051	0.0026	0.1257	0.8589	Qinhuangdao	0.0429	0.0008	0.0010	0.0485	0.1011
Changzhou	0.1378	0.0010	-0.0007	0.1265	-0.2037	Quanzhou	0.0225	-0.0013	-0.0021	0.0111	-0.2045
Chifeng	0.0194	-0.0015	-0.0010	0.0043	-0.2706	Rizhao	0.1251	0.0000	-0.0020	0.0925	-0.5865
Dezhou	0.1161	0.0025	0.0026	0.1465	0.5474	Shanghai	0.1235	0.0011	0.0008	0.1330	0.1699
Dongguan	0.0619	0.0002	0.0018	0.0864	0.4399	Shangqiu	0.1688	0.0005	-0.0024	0.1353	-0.6034
Dongying	0.1212	0.0012	0.0017	0.1635	0.7598	Shantou	0.0359	-0.0001	-0.0013	0.0249	-0.1974
Foshan	0.0922	0.0021	0.0013	0.1184	0.4710	Shaoxing	0.0925	0.0004	-0.0012	0.0743	-0.3277
Fuyang	0.0876	0.0007	-0.0014	0.0637	-0.4297	Shenyang	0.0920	0.0043	0.0018	0.1905	1.7732
Fuzhou	0.0714	-0.0009	-0.0020	0.0539	-0.3135	Shenzhen	0.0164	0.0001	0.0048	0.0240	0.9598
Guangzhou	0.0272	0.0474	0.0013	0.9368	0.2802	Suqian	0.1540	-0.0008	-0.0034	0.0856	-1.2321
Handan	0.1416	0.0026	-0.0011	0.1351	-0.1183	Suzhou	0.1447	0.0015	-0.0001	0.1413	-0.0616
Hangzhou	0.0955	-0.0001	-0.0013	0.0768	-0.3363	Taian	0.0739	0.0007	0.0014	0.1076	0.6065
Hohhot	0.0303	0.0020	0.0010	0.0529	0.4056	Taiwan	0.0288	0.0002	0.0017	0.0414	0.2283
Hongkong	-0.0142	-0.0001	0.0036	0.0101	0.4371	Taiyuan	0.0379	0.0037	0.0034	0.1100	1.2976
Huizhou	0.0020	-0.0009	0.0006	0.0086	0.1188	Taizhou	0.0593	-0.0005	-0.0020	0.0414	-0.3217
Huzhou	0.1204	-0.0003	-0.0024	0.0645	-1.0074	Taizhou	0.1210	-0.0001	-0.0043	0.0824	-0.6959

Jiamusi	-0.0412	-0.0029	0.0004	-0.0248	0.2961	Tangshan	0.1034	0.0009	0.0002	0.1130	0.1732
Jiangmen	0.0264	0.0010	0.0010	0.0423	0.2852	Urumqi	0.0765	0.0019	0.0016	0.1337	1.0292
Jieyang	0.0489	-0.0005	-0.0032	0.0047	-0.7953	Wenzhou	0.0497	0.0005	-0.0008	0.0348	-0.2687
Jilin	-0.0159	-0.0015	0.0007	0.0102	0.4707	Wuxi	0.1289	0.0008	0.0005	0.1424	0.2427
Jinan	0.0751	0.0019	0.0024	0.1126	0.6760	Xi’an	0.1155	0.0017	-0.0003	0.1012	-0.2566
Jining	0.1385	0.0004	-0.0008	0.1293	-0.1662	Xiamen	0.0267	-0.0014	-0.0032	-0.0048	-0.5672
Jinzhong	0.0659	0.0037	0.0021	0.1392	1.3192	Xingtai	0.1191	0.0026	0.0005	0.1268	0.1385
Karamay	0.0554	0.0015	0.0022	0.1805	2.2527	Xuzhou	0.1355	-0.0005	-0.0022	0.1153	-0.3644
Kashgar	0.0876	0.0018	-0.0009	0.0676	-0.3601	Yancheng	0.1484	-0.0010	-0.0031	0.1035	-0.8081
Kunming	0.0008	-0.0006	-0.0027	-0.0195	-0.3661	Yinchuan	0.0816	0.0016	0.0020	0.1679	1.5538
Langfang	0.1190	0.0017	0.0005	0.1228	0.0680	Zhangjiagang	0.0021	0.0025	0.0015	0.0534	0.9225
Lianyungang	0.1190	0.0002	-0.0010	0.1072	-0.2124	Zhengzhou	0.1797	0.0021	-0.0021	0.1410	-0.6979
Liaocheng	0.1464	0.0020	0.0009	0.1703	0.4312	Zhongshan	0.0639	0.0005	0.0001	0.0822	0.3300
Liaoyang	0.0903	0.0038	0.0018	0.2009	1.9895	Zhuhai	0.0179	0.0005	0.0020	0.0224	0.0810
Linxi	0.1409	0.0003	-0.0003	0.1312	-0.1755	Zibo	0.1182	0.0014	0.0013	0.1331	0.2671
Luoyang	0.1219	0.0012	-0.0011	0.0915	-0.5478						

Supplementary Table 4 | Detailed description of data.					
Data name	**Spatial resolution**	**Time resolution**	**Source**	**Unit**	**Note**
Administrative division	1: 1 million	2015	NCSGI.a	/	Basic base map data
MOD13A2	1000 m	16-Day	USGS.b	/	UG index
MCD12Q1	500 m	Annual	USGS.b	/	Accuracy verification of Global Urban Boundaries data
MOD11A1	1000 m	Daily	USGS.b	Kelvin	UST index
MOD09A1	500 m	8-Day	USGS.b	/	Calculate IBI index
ERA5-Land reanalysis dataset	10000 m	Day	ECMWF.c	/	Sensitivity analysis
Population density datasets	1000 m	Annual	WorldPop.d	/	Sensitivity analysis
Impervious surface data	30 m	Annual	Paper [24]		
Harmonized lobal nighttime light dataset	1000 m	Annual	Paper [25]	/	Sensitivity analysis
China's high-resolution eco-environmental quality	1000 m	Annual	NESSDC. e	/	Eco-environmental benefits analysis
Global Urban Boundaries	30 m	Annual	Paper [14]	/	Delineate LUBs

Note: a, National Catalogue Service for Geographic Information (https://www.webmap.cn/). b, United States Geological Survey (https://earthexplorer.usgs.gov/). c, European Centre for Medium-Range Weather Forecasts (https://www.ecmwf.int/). d, WordPop (https://www.worldpop.org/). e, National Earth System Science Data Center (http://www.geodata.cn/).

Abbreviations:

UST, urban surface temperature

UG, urban greening

UI, urban impermeability

LUB, largest urban boundaries

MUB, main urban boundaries

GUB, grown urban boundaries

CPUG, cooling potential of urban greening

Sen_UST, change trend of UST based on the Theil-Sen median

Sen_NDVI, change trend of NDVI based on the Theil-Sen median

Sen_IBI, change trend of IBI based on the Theil-Sen median

ERP, ecological restoration project

References

1. Campbell I, Sachar S, Meisel J, et al. Beating the heat: A sustainable Cooling Handbook for Cities[M]. United Nations Environment Programme, 2021.

2. Sun L, Chen J, Li Q, et al. Dramatic uneven urbanization of large cities throughout the world in recent decades[J]. Nature communications, 2020, 11(1): 1-9.

3. Estoque, Ronald C., Yuji Murayama, and Soe W. Myint. "Effects of landscape composition and pattern on land surface temperature: An urban heat island study in the megacities of Southeast Asia." Science of the Total Environment 577 (2017):

4. Xu C, Dong L, Yu C, et al. Can forest city construction affect urban air quality? The evidence from the Beijing-Tianjin-Hebei urban agglomeration of China[J]. Journal of Cleaner Production, 2020, 264: 121607.

5. Wang Z, Bai T, Xu D, et al. Temporal and Spatial Changes in Vegetation Ecological Quality and Driving Mechanism in Kökyar Project Area from 2000 to 2021[J]. Sustainability, 2022, 14(13): 7668.

6. Missall S, Welp M, Thevs N, et al. Establishment and maintenance of regulating ecosystem services in a dryland area of central Asia, illustrated using the Kökyar Protection Forest, Aksu, NW China, as an example[J]. Earth System Dynamics, 2015, 6(1): 359-373.

7. Li Y, Li Y, Zhou Y, et al. Investigation of a coupling model of coordination between urbanization and the environment[J]. Journal of environmental management, 2012, 98: 127-133.

8. Gramsci and Marxist Theory (RLE: Gramsci)[M]. Routledge, 2014.

9. Gu C. Urbanization: Processes and driving forces[J]. Science China Earth Sciences, 2019, 62(9): 1351-1360.

10. Xu H. A remote sensing index for assessment of regional ecological changes[J]. China Environmental Science, 2013, 33(5): 889-897.

11. Liao W, Jiang W. Evaluation of the Spatiotemporal Variations in the Eco-environmental Quality in China Based on the Remote Sensing Ecological Index[J]. Remote Sensing, 2020, 12(15): 2462. 10.3390/rs12152462

12. HJ 192-2015, Technical Criterion for Ecosystem Status Evaluation[S].

13. Zheng K, Wei J Z, Pei J Y, et al. Impacts of climate change and human activities on grassland vegetation variation in the Chinese Loess Plateau[J]. Science of the Total Environment, 2019, 660: 236-244.

14. Li X, Gong P, Zhou Y, et al. Mapping global urban boundaries from the global artificial impervious area (GAIA) data[J]. Environmental Research Letters, 2020, 15(9): 094044.

15. Chen J, Gao M, Cheng S, et al. Global 1 km× 1 km gridded revised real gross domestic product and electricity consumption during 1992–2019 based on calibrated nighttime light data[J]. Scientific Data, 2022, 9(1): 1-14.

16. Zhou, Weiqi, et al. "Relationships between land cover and the surface urban heat island: seasonal variability and effects of spatial and thematic resolution of land cover data on predicting land surface temperatures." Landscape ecology 29.1 (2014): 153-167.

17. Tayyebi, Amin, Phillips Christian Perry, and Amir Hossein Tayyebi. "Predicting the expansion of an urban boundary using spatial logistic regression and hybrid raster–vector routines with remote sensing and GIS." International Journal of Geographical Information Science 28.4 (2014): 639-659.

18. Li X, Gong P, Zhou Y, et al. Mapping global urban boundaries from the global artificial impervious area (GAIA) data[J]. Environmental Research Letters, 2020, 15(9): 094044.

19. Zheng, Jingyun, Yunhe Yin, and Bingyuan Li. "A new scheme for climate regionalization in China." Acta Geographica Sinica 65.1 (2010): 3-12.

20. Alkama R, Cescatti A. Biophysical climate impacts of recent changes in global forest cover[J]. Science, 2016, 351(6273): 600-604.

21. Liu J, Kuang W, Zhang Z, et al. Spatiotemporal characteristics, patterns, and causes of land-use changes in China since the late 1980s[J]. Journal of Geographical sciences, 2014, 24: 195-210.

22. Cool Coalition. BEATING THE HEAT: A SUSTAINABLE COOLING HANDBOOK FOR CITIES[R]. U.K: Glasgow, 2012.

23. Dinda S. Environmental Kuznets curve hypothesis: a survey[J]. Ecological economics, 2004, 49(4): 431-455.

24. Gong P, Li X, Wang J, et al. Annual maps of global artificial impervious area (GAIA) between 1985 and 2018[J]. Remote Sensing of Environment, 2020, 236: 111510.

25. Li X, Zhou Y, Zhao M, et al. A harmonized global nighttime light dataset 1992–2018[J]. Scientific data, 2020, 7(1): 1-9.